Implantable Neural Probes with Monolithically Integrated CNTFET Arrays for Multimodal Monitoring

Jie Xia[1], Luxi Zhang[1], Shengming Wang[1], Yanlan Yu[2], Li Ding[3], Fan Zhang[1], Shaomin Zhang[1], Jikui Luo[1], Yan Yan Shery Huang[4], Luigi Occhipinti[4], Gang Pan[1*], Zhen Cao[1,5*], Guoqing Ding[2*], Shurong Dong[1,2*]

[1] The State Key Lab of Brain-Machine Intelligence, Zhejiang University, Hangzhou 310027, China
[2] Department of Urology of Sir Run Shaw Hospital, Hangzhou, 310027, China
[3] Key Laboratory for the Physics and Chemistry of Nanodevices and Center for Carbon-based Electronics, Department of Electronics, Peking University, Beijing, China
[4]Department of Engineering, University of Cambridge, Cambridge, CB3 0FA UK.
[5] Zhejiang Provincial Engineering Research Center of Innovative Instruments for Precise Pathogen Detection, Hangzhou, China

[*]**Correspondence:**

gpan@zju.edu.cn;

eezcao@zju.edu.cn;

3196014@zju.edu.cn;

dongshurong@zju.edu.cn

This file contains:

Supplementary Figures 1–14

Supplementary Tables 1–4

Supplementary References

Supplementary Information

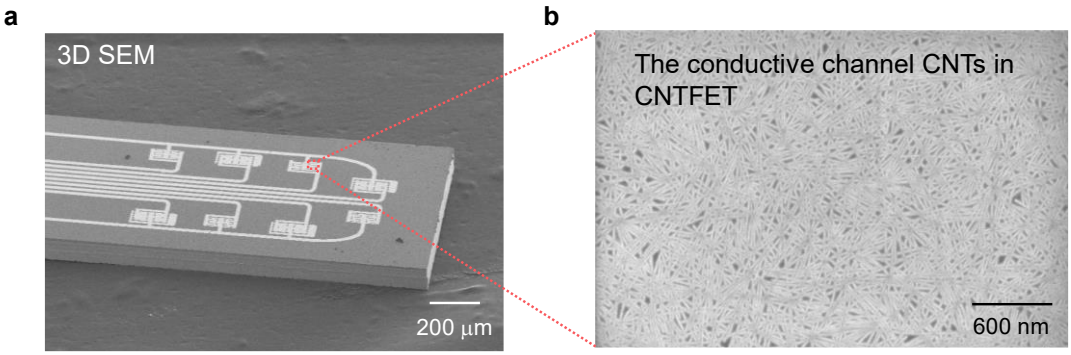

Supplementary Fig. 1. SEM image of MICA-NP. (a) The 3D SEM image of the front end of the MICA-NP (EHT = 5.00 kV, WD = 9.7 mm, Mag = 49 X). (b) The SEM image of CNTs (EHT = 1.00 kV, WD = 4.1 mm, Mag = 28.97 K X).

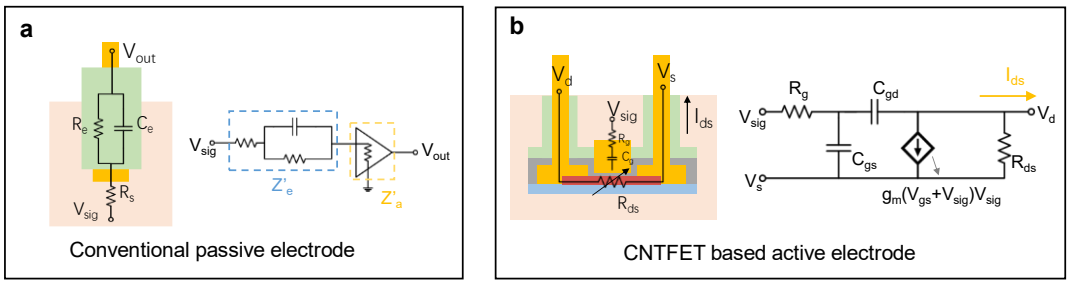

Supplementary Fig. 2. The comparison between the conventional passive electrode and the MICA-NP. Equivalent circuit model based on (a) the conventional passive electrode and (b)the MICA-NP.

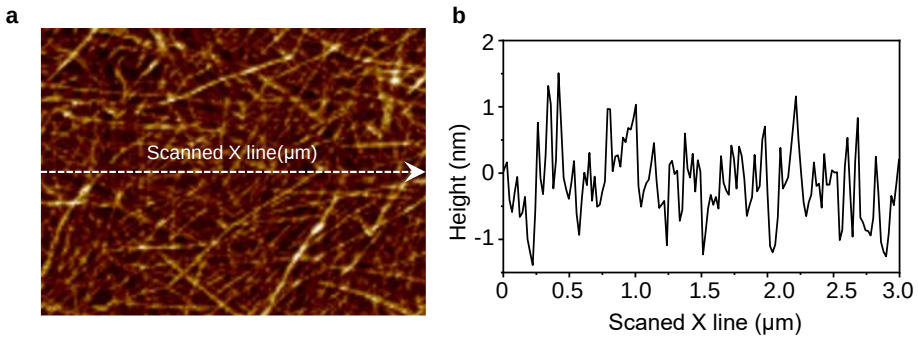

Supplementary Fig. 3. AFM image and height distribution of CNTs. (a) The AFM image of SWCNTs films with height scanning *line X*. (b) The height distribution on *line X* shows that the transistor channel layer is a monolayer with a thickness of about 2 nm.

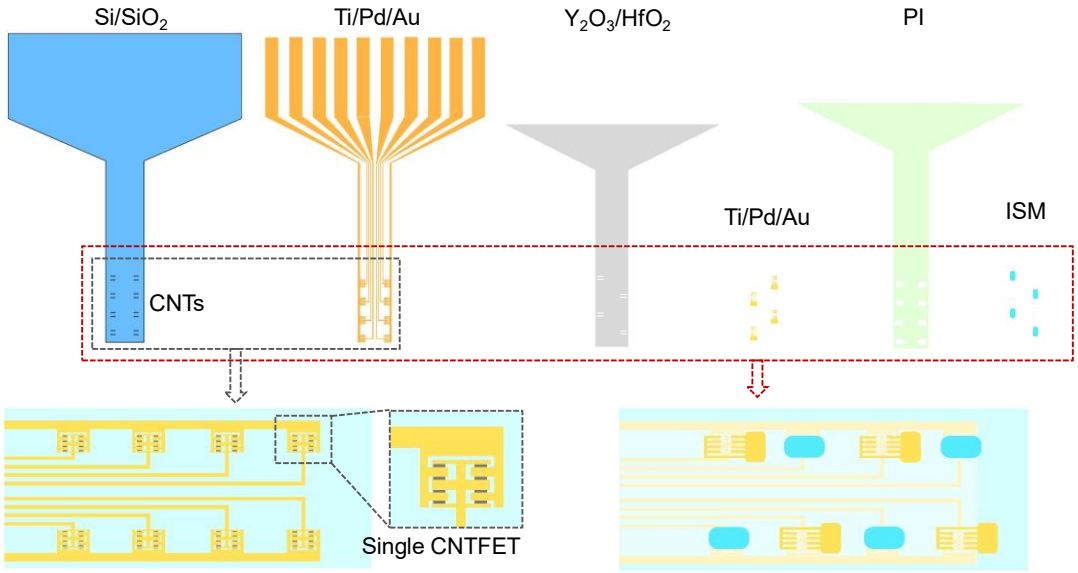

Supplementary Fig. 4. The fabrication process of the MICA-NP. CNTs were deposited on a lightly doped p-type 4-inch, 100-μm silicon wafer, pre-coated with 300 nm SiO_2, using a solution-based deposition method. The active CNT regions were etched using ICP-RIE. The source and drain electrodes of the CNTFET were fabricated through photolithography and lift-off. The CNT channel, with a total length of 5 μm (3 μm active length, 1 μm each in contact with the source and drain), a width of 20 μm, and 8 interpolations, was defined. A Ti/Pd/Au (0.3/20/40 nm) metal layer was sputtered onto the patterned substrate and then immersed in acetone to remove excess metal. Y_2O_3 (4 nm) and HfO_2 (5 nm) were deposited as the gate insulator using ALD. The gate was defined using photolithography and lift-off with Ti/Pd/Au (0.3/20/40 nm). A 3 μm thick polyimide encapsulation layer was deposited by CVD and then MICA-NPs were individually cut using the laser scribing method. Ultimately, Ca^{2+}-ISM was coated on the CNTs to monitor Ca^{2+} concentration changes.

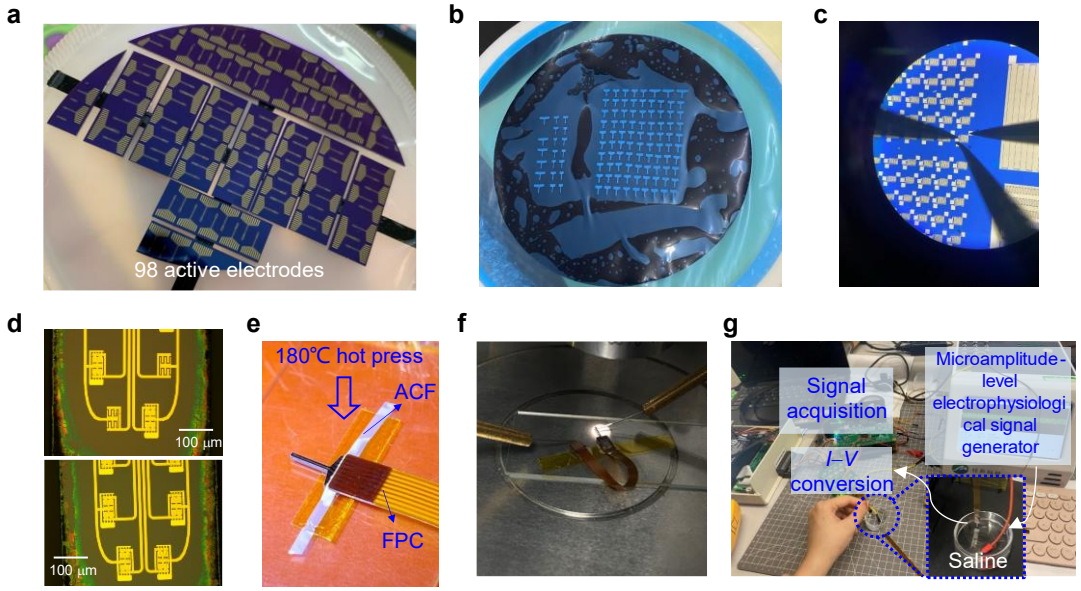

Supplementary Fig. 5. The mass production efficiency of electrodes and the performance testing of transistors are shown. (a) Half a four-inch piece of silicon has an effective number of 89 electrodes. (b) The brain electrodes are cut by a laser with a linewidth of 5 μm. (c) The CNTFET performance is most realistically assessed by testing a single transistor with source, drain, and gate PAD. (d) The front end of the laser-cut brain electrode transistor is intact. (e) Bonding electrodes to the flexible printed circuit (FPC) using anisotropic conductive film (ACF) under hot pressing. (f) The bonding electrodes were tested by a probe station. (g) Brain electrodes were tested with saline in vitro.

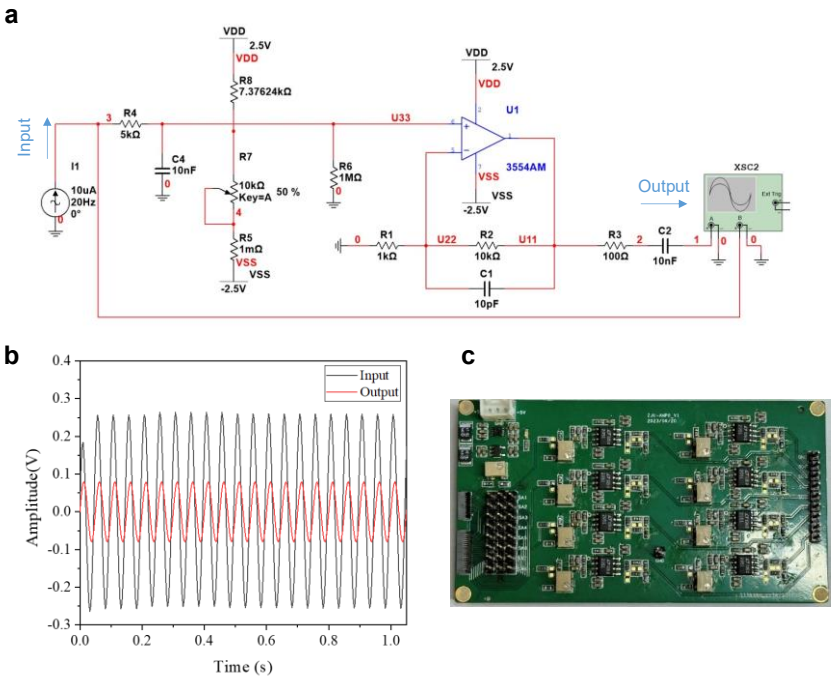

Supplementary Fig. 6. *I–V* conversion circuit. (a) The *I–V* conversion circuit diagram. (b) The simulation data output of (a). (c) The photograph of the *I–V* circuit board.

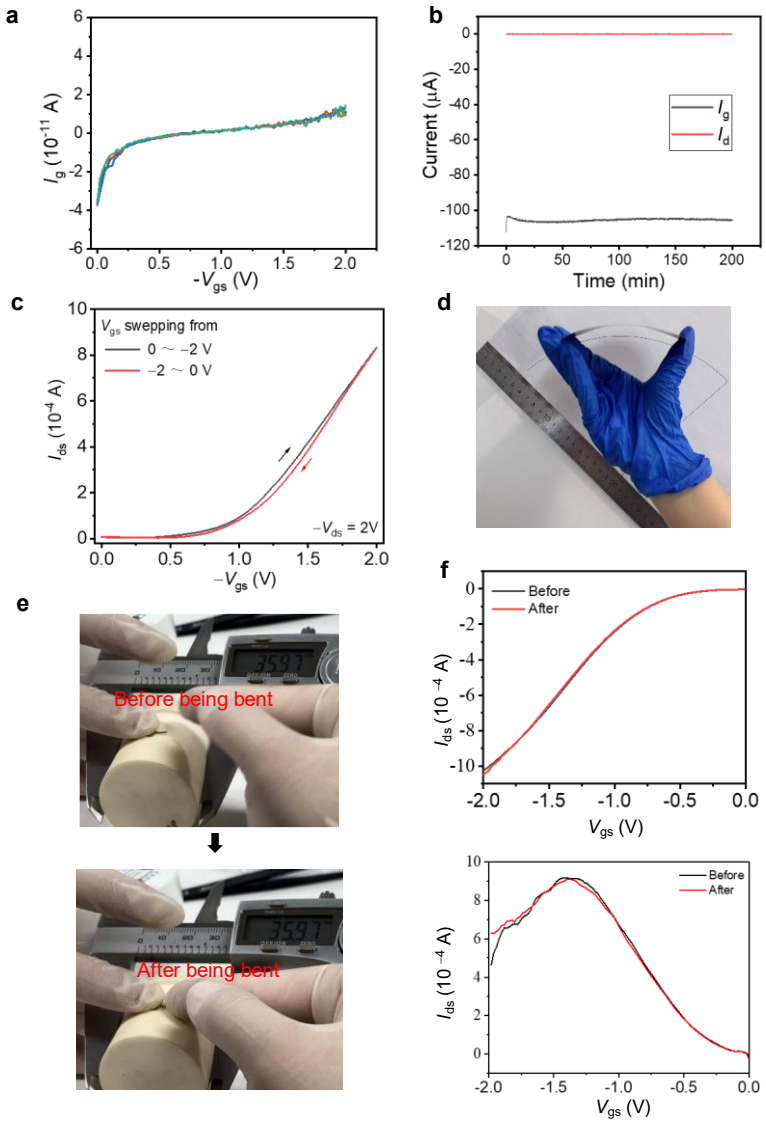

Supplementary Fig. 7. Performance characterization of MICA-NP (a) Input curve of the electrode. (b) Transistor long time stability curve. (c) Back-and-forth scanning of transmission curves of CNTFETs (cyclic sweeps of gate voltage 0 V to –2 V and –2 V to 0 V). (d) Mechanical durability of the MICA-NPs were tested by bending 100 times whit a radius of curvature of 15 cm. (e) The MICA-NP was bent with a radius of 18 mm. (f) transmission curve and transconductance curves of CNTFET before and after being bent bent with a radius of 18 mm.

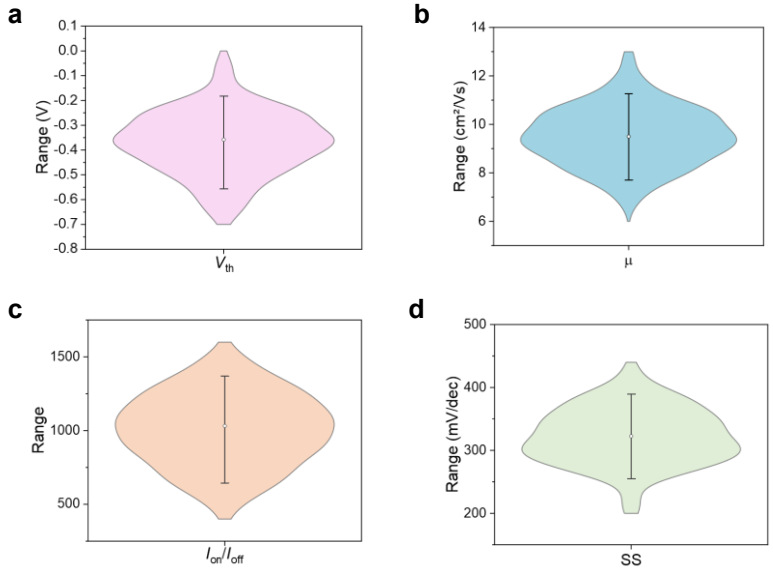

Supplementary Fig. 8. Eighty transistors are randomly selected to calculate their performance. (a) The average V_{th} value is 0.35 V. (b) The average carrier mobility (μ) is 11.89 cm^2/Vs. (c) The current switching ratio I_{on}/I_{off} is 1268.8. (d) and the subthreshold swing (SS) is 330.96 mV/dec ('°' is the mean value in images, with a range of 5% to 95% in parentheses).

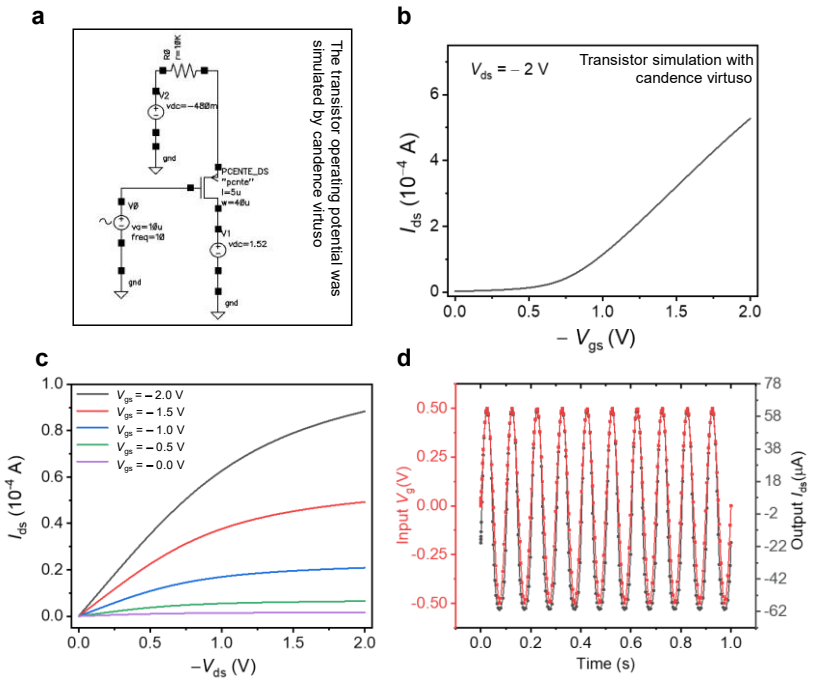

Supplementary Fig. 9. Transistor simulation. cadence virtuso simulated CNTFET by lower Text, and add the bias circuit as shown in (a). The simulated transistor transmission curve (b), output curve (c), and tested the sine-wave signal detection capability (d) at the working point.

The text of Supplementary Fig. 9. Transistor simulation code using cadence virtuso

```
// "spectre" description for "pkucnt_mysch", "cntmodel", "spectreText"
simulator lang=spice insensitive=yes
.model pcnte pmos level=62
+ rd=3000 rdx=0.0 rs=3000 rsx=0.0
+ cgdo=0 cgso=0 etac0=52 etac00=52    mc=3.0
+ lkink=0 mk=1.3 vkink=9.1
+ i0=1e-10 blk=1e-3 dd=1.0 dg=2.0e-6 i00=150 eb=0.568
+ asat=1.2 eta=14 mus=40.0
+ mu0=20 mu1=0.02 mmu=2
+ vto=-1 delta=4 VST=9 VSI=15 at=20e-10
+ tnom=27 tox=30e-9 vfb=0
```

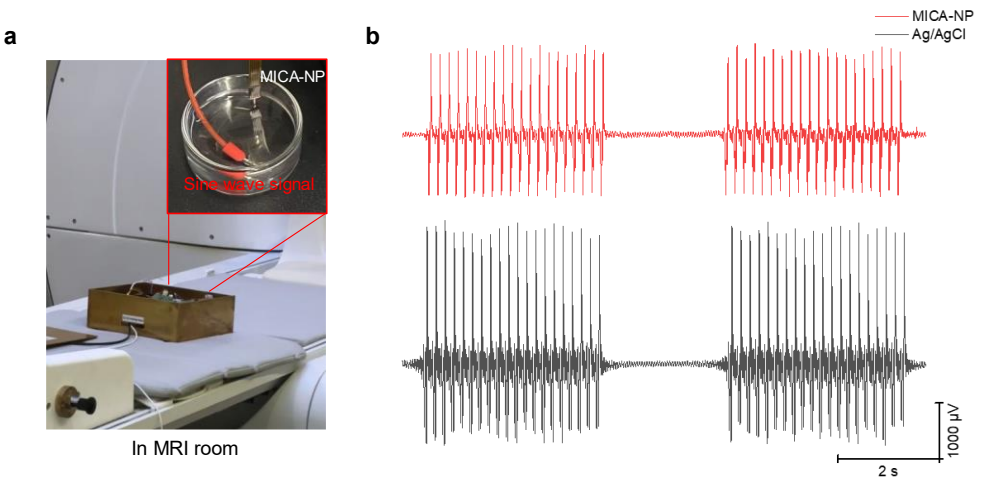

Supplementary Fig. 10. Compared the signal acquisition ability of MICA-NP and Ag/AgCl electrodes in MRI. (a) Faraday cage is formed by copper shell to reduce the influence of nuclear magnetism on acquisition module. The red line inputted the sine wave signal to the positive end of the signal generator. The ground end of the signal generator and the ground end of the I-V converter board are connected together in a copper shield box. (b) The signal generator generated 20 Hz 20 μV sine wave signal and applied it to 0.9% normal saline, while MICA-NP and Ag/AgCl electrodes collected signal from saline. Diffusion weighted imaging scanning was performed on MRI. TR duration was 3235 ms, TE duration was 88ms, and TR was divided into 20 echo planar imaging segments.

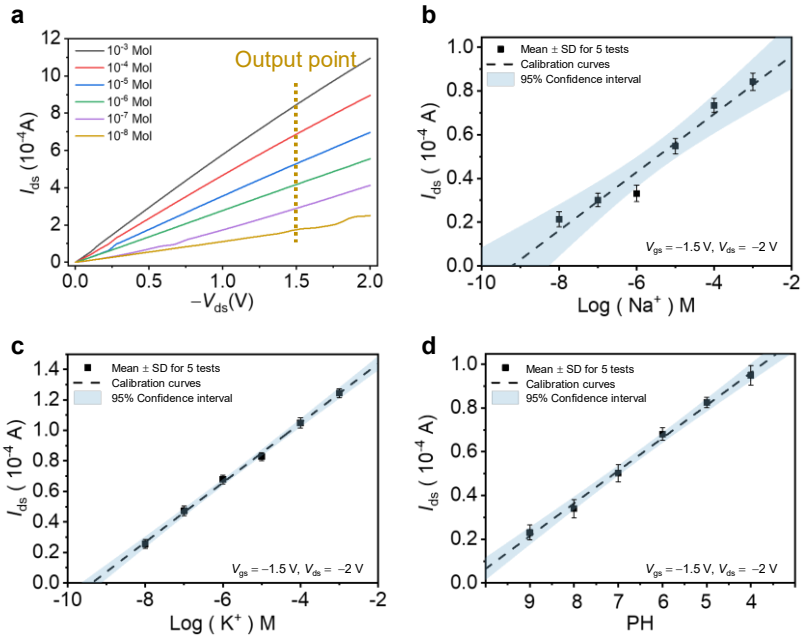

Supplementary Fig. 11. Calcium ion detection *in Vitro*. (a) Output curves of Ca^{2+} sensor under different Ca^{2+} concentrations while V_{gs} = −1.5 V. (b–d) Response curves of the Ca^{2+} sensors to Na^+, K^+, and PH in solution, respectively. The error line is the SD of N = 5 FETs.

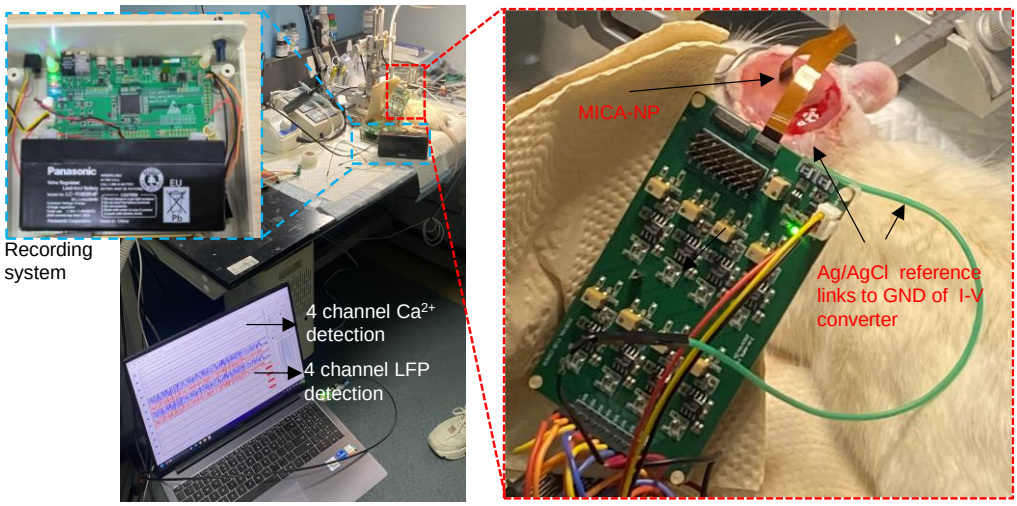

Supplementary Fig. 12. Detection system and experiment set-up. The specific electrode connection and collection process for using the MICA-NP into the target brain region of mice to assess the ability of LFP recordings. The recording system is reported at Jiadong P. *et al.*[9].

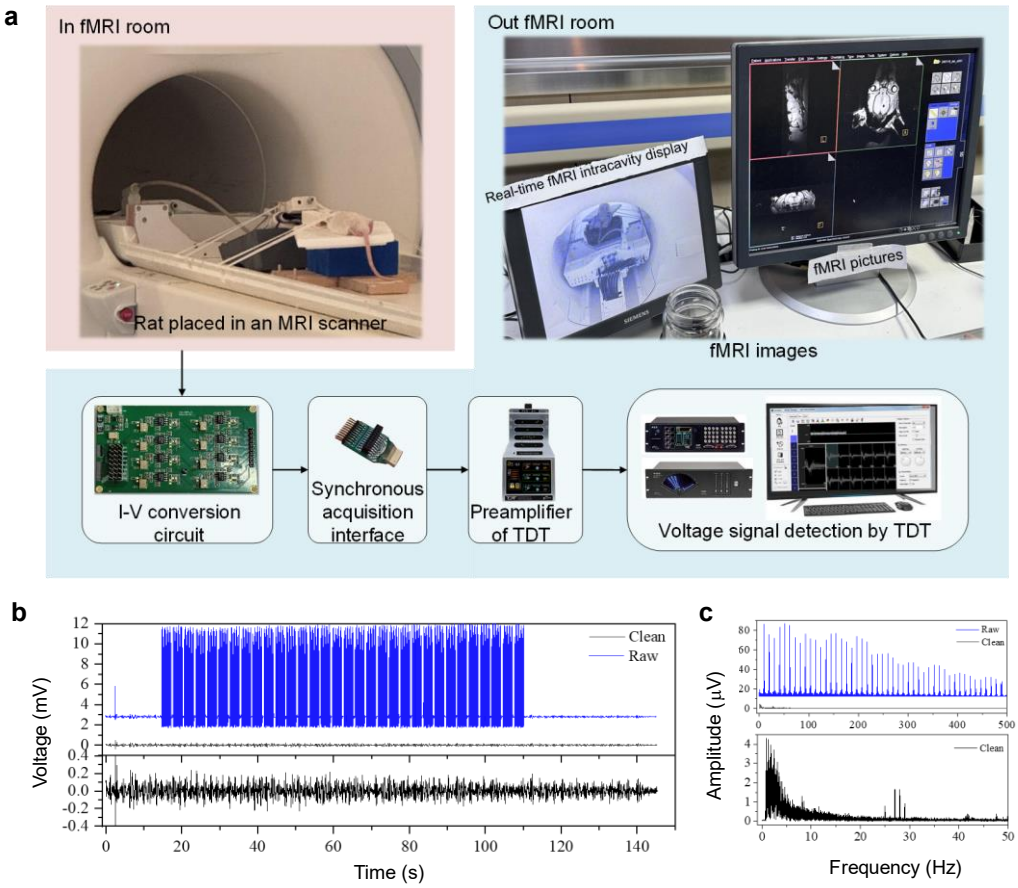

Supplementary Fig. 13. *In Vivo* monitoring of multimodal brain activity with MICA-NP (a) Schematic diagram of LFP acquisition process using electrodes under 7T nuclear magnetic scanning. (b) A volume of EPI scans, containing 32 slices, and EEG signals after removing GA. (c) The spectrum of LFP with GA in (b, top), and the spectrum of LFP without GA interference (bottom).

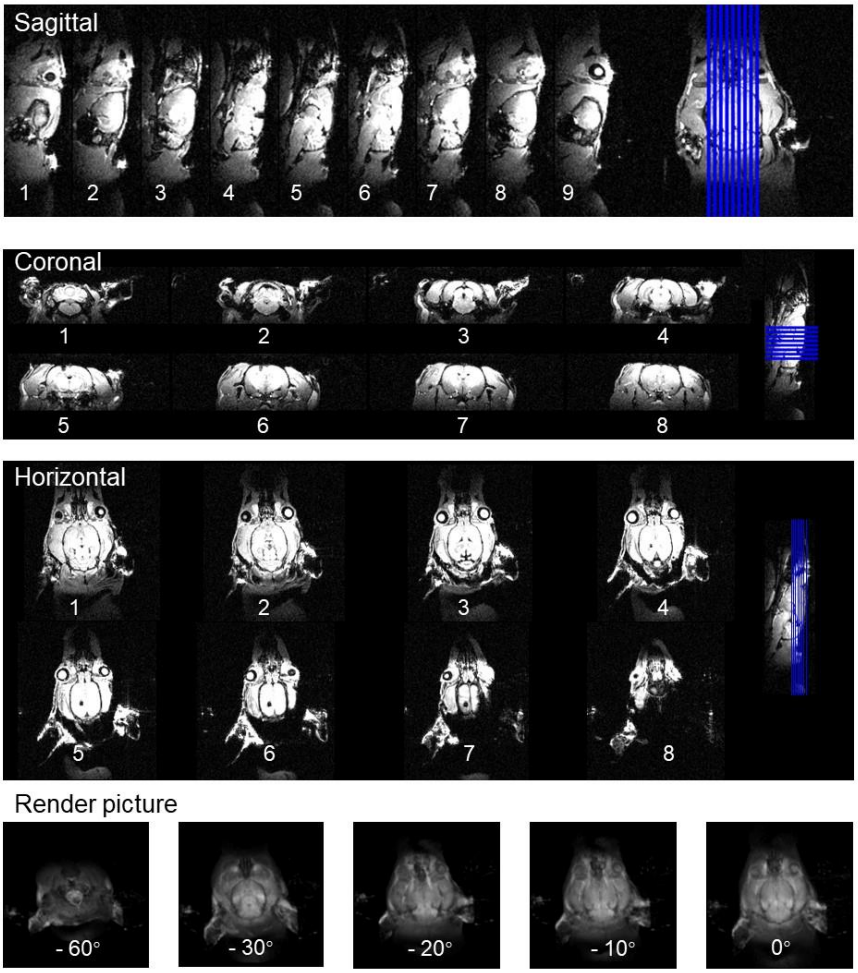

Supplementary Fig. 14. MRI images of a rat's brain following MICA-NP implantation. T1-weighted MRI slice at various depth of a rat's brain from sagittal, coronal, and horizontal dimensions. And three-dimensional images of rat's brain rendered from upper MRI images in three dimensions (56 slices).

Supplementary Table 1 | Comparison of the characteristics of our MICA-NP and other transistors for brain electrode applications.

Active/ passive	Type	Transistors/materials	Mobility	Transconductance	Size of FET	Frequency response	SNR	Ref.
Active	ECoG	ZnO TFTs	/	6.8 μS	3.6 × 1.75 mm^2	0.2 Hz-32 kHZ	32.2 dB	[1]
Active	ECoG (SGFETs)	Graphene	863 cm^2/Vs	2.2 mS	300 × 300μm^2	up to 1 kHz	13 dB	[2]
Active	Probe (SGFETs)	Graphene	/	1.1 mS	60 × 100 μm^2	up to 5 kHz	1-40 dB	[3]
Active	ECoG	PEDOT:PSS	/	11 mS	120 × 120 μm^2	/	48 dB (epilepsy)	[4]
Active	**Probe**	**CNTs**	**11.89 cm^2/Vs**	**91 μS**	**50 × 147 μm^2**	**0.01 Hz–32 kHZ**	**40.34 dB**	**Our work**

Supplementary Table 2 | Comparison of the characteristics of our MICA-NP and other devices for Ca^{2+} detection.

Electrode	Type	Sensitivity	Detection range	Multimodels	Ref.
SGFET with graphene on hBN	Active; Out of brain	-71 mV/dec	10^{-4}-10^{0} M	K^+, Na^+, Ca^{2+}	[5]
ECoG based on carbon nanotube array	Passive; ECoG	28.86 mV/dec	10^{-5}-10^{-2} M	LFP, K^+, Na^+, Ca^{2+}	[6]
Tungsten microelectrode with ion-selective membrane	Passive; Microarray probe;	26.5 ± 2.9 mV/dec	10^{-3} – 10^{-1} M	LFP, K^+, Na^+, Ca^{2+}	[7]
Platinum black	Passive; Probe	100.7 mV/dec	10^{-4} – 10^{-3} M	LFP, Ca^{2+}	[8]
MICA-NP	Active; Probe	**128.78 μA/dec**	**10^{-8} - 10^{-3} M**	**LFP, Ca^{2+}, 7.0 T MRI compatible**	**Our work**

Supplementary Table 3 | Comparison of the characteristics of our MICA-NP and other electrodes for magnetic compatibility.

Electrode	Type	Size of contact	Electrical properties	Artifacts detected	Ref.
Parylene-C-insulated CNT fiber electrode	Passive electrode; Probe	10–25 μm in diameter	(20-μm CNT fiber treated with nitric acid)；Impedance was 279.96 ± 32.08 kΩ at 1 kHz; CSC was 419.87 ± 73.04 mC/cm^2; CIL was 5.04 ± 0.22 mC/cm^2	(20-μm single CNT fiber) artifact size of 268.4 ± 29.9 μm in T2-weighted anatomical images at 7.0 T (*in vivo*)	10
Graphene fiber electrodes	Passive electrode; Probe	0.17 mm in diameter	Impedance was 15.1 ± 3.67 kΩ at 1 kHz; CSC was 889.8 ± 158.0 mC cm^{-2}; CIL was 10.1 ± 2.25 mC cm^{-2}	~0.18 ± 0.04 mm artifacts in diameter in T2 anatomical images, ~0.70 ± 0.05 mm in EPI at 9.4 T (*in vivo*)	11
Gold-aluminum microwire neural electrodes	Passive electrode; Probe	Two 100-μm Au wires and two 125-μm AI wires twisted together	Conductance was over 2 $M\Omega^{-1}$	Up to 0.85 mm artifacts in GEMS and up to 1.25 mm in GRE-EPI (*in vivo*)	12
Graphene grown on a patterned Mo	Passive electrode; Probe	340 × 200 μm^2	Impedance at 1 kHz was measured to be 27.4 kΩ	CVD graphene electrodes did not cause any image artifacts in a 3T MRI scanner	13
PEDOT:PSS (Poly(3,4-ethylenedioxythiophene) polystyrene sulfonate)	Passive electrode; Probe	250 × 250 μm^2 with a fill factor of 30%	Impedance values at 1 kHz were 14.64 kΩ–19.34 kΩ	The PEDOT:PSS optimized open-mesh electrode showed completely artifact-free images in MRI scans	14
MICA-NP	**Active electrode; Probe**	**50×147 μm^2**	**The LFPs were converted into current through CNTFETs within the MRI cavity, and then be processed in the shielding box；SNR up to 40.34 dB**	**MICA-NP did not cause any image artifacts in a 7T MRI scanner**	**Our work**

Supplementary Table 4 | Comparison of the advantages and disadvantages of our MICA-NP and other multimodal or active brain electrodes.

Electrode	Function	Application	Advantage	Disadvantage	Ref.
PEDOT:PSS-based conformal brain implants	LFPs recording; MRI compatible	LFPs recording during 1 Hz electrical stimulation on rat's S1 area	Good biocompatibility; Small artifacts;	Passive electrode; Lack SNR of spontaneous LFPs; Missing information of impedance and frequency response;	[15]
Electrochemophysiological microarray	K^+, Ca^{2+}, Na^+, and pH detection; LFPs recording	Seizure in rats	Multiple detection functions;	Rigid electrode array; Passive electrode;	[16]
CNT-based ECoG	Ca^{2+}, K^+, and Na^+ detection; LFPs recording	Seizure in rats	Multiple detection functions;	Passive electrode; Large electrode size; Lack of *in vivo* use;	[17]
Graphene solution-gated field-effect transistors based ECoG	LFPs recording	Cortical spreading depression; Ultraslow or infra slow activity	Full-band response(<10kHz); Active electrode; Two dimensional EEG map;	Unable to detect brain ion concentration; Magnetic incompatibility	[18]
Graphene depth neural probes	LFPs recording	Seizure in rats	Full-band response; Active electrode;	Unable to detect brain ion concentration; Magnetic incompatibility	[3]
MICA-NP	**LFPs recording; Ca^{2+}detection; 7.0 T MRI compatible;**	**Seizure state in rats**	**0.01 Hz–32 kHz frequency response; Active electrode; Multiple functions; 7.0 T MRI compatible**	**More applications need to be explored;**	**Our work**

Supplementary References

1. Zhang, F. et al. Multimodal electrocorticogram active electrode array based on zinc oxide-thin film transistors. *Adv. Sci.* **10**, 2204467 (2023).

2. Hébert, E. et al. Inkjet-Printed, Flexible organic electrochemical transistors for high-performance electrocorticography recordings. *Adv. Func. Mater.* **28**, 1703976 (2018).

3. Bonaccini, C. A. et al. Full-bandwidth electrophysiology of seizures and epileptiform activity enabled by flexible graphene microtransistor depth neural probes. *Nat. Nanotech.* **17**, 301-309 (2022).

4. Khoury, F. et al. Inkjet-printed, flexible organic electrochemical transistors for high-performance electrocorticography recordings. *ACS Appl. Mater. Interfaces* **16**, 55045-55055 (2024).

5. Hasan, N. et al. Ion-selective membrane-coated graphene–hexagonal boron nitride heterostructures for field-effect ion sensing. *ACS Omega* **6**, 30281-30291 (2021).

6. Yang, H. et al. Carbon nanotube array‐based flexible multifunctional electrodes to record electrophysiology and ions on the cerebral cortex in real time. *Adv. Func. Mater.* **32**, 2204794 (2022).

7. Zhao, F. et al. An electrochemophysiological microarray for real‐time monitoring and quantification of multiple ions in the brain of a freely moving rat. *Angew. Chem.* **132**, 10512-10516 (2020).

8. Xiao, J. et al. Implantable probe with integrated reference electrode for in situ neural signal and calcium ion monitoring. *Bio-Des. Manuf.* **7**, 591-595 (2024).

9. Pan, J. et al. 7T magnetic compatible multimodality electrophysiological signal recording system. *Electronics* **12**, 3648 (2023).

10. Lu, L. et al. Soft and mri-compatible neural electrodes from carbon nanotube fibers. *Nano Lett.* **19**, 1577-1586 (2019).

11. Zhao, S. et al. Full activation pattern mapping by simultaneous deep brain stimulation and fmri with graphene fiber electrodes. *Nat. Commun.* **11**, 1788 (2020).

12. Cruttenden, C. E. et al. Novel composite gold-aluminum electrode with application to neural recording and stimulation in ultrahigh field magnetic resonance imaging scanners. *Ann. Biomed. Eng.* **49**, 2337-2348 (2021).

13. Bakhshaee, B. N. et al. Multilayer cvd graphene electrodes using a transfer-free process for the next generation of optically transparent and mri-compatible neural interfaces. *Microsyst. Nanoeng.* **8**, 107 (2022).

14. Hong, J. H. et al. Monolayer, open-mesh, pristine pedot: pss-based conformal brain implants for fully mri-compatible neural interfaces. *Biosens. Bioelectron.* **260**, 116446 (2024).

15. Hong, J. H. et al. Monolayer, open-mesh, pristine pedot: pss-based conformal brain implants for fully mri-compatible neural interfaces. *Biosens. Bioelectron.* **260**, 116446 (2024).

16. Zhao, F. et al. An electrochemophysiological microarray for real‐time monitoring and quantification of multiple ions in the brain of a freely moving rat. *Angew. Chem.* **132**, 10512-10516 (2020).

17. Yang, H. et al. Carbon nanotube array‐based flexible multifunctional electrodes to record electrophysiology and ions on the cerebral cortex in real time. *Adv. Func. Mater.* **32**, 2204794 (2022).

18. Masvidal, C. E. et al. High-resolution mapping of infraslow cortical brain activity enabled by graphene microtransistors. *Nat. Mater.* **18**, 280-288(2019).